

PAPER • OPEN ACCESS

Fubini–Study metric and topological properties of flat band electronic states: the case of an atomic chain with $s - p$ orbitals

To cite this article: Abdiel de Jesús Espinosa-Champo and Gerardo G Naumis 2024 *J. Phys.: Condens. Matter* **36** 015502

View the [article online](#) for updates and enhancements.

You may also like

- [Quantum Monte Carlo study of hard-core bosons in Creutz ladder with zero flux](#)
Yang Lin, , Weichang Hao et al.
- [Creutz ladder in a resonantly shaken 1D optical lattice](#)
Jin Hyoun Kang, Jeong Ho Han and Y Shin
- [Compactly supported Wannier functions and strictly local projectors](#)
Pratik Sathe, Fenner Harper and Rahul Roy

Fubini–Study metric and topological properties of flat band electronic states: the case of an atomic chain with $s - p$ orbitals

Abdiel de Jesús Espinosa-Champo  and Gerardo G Naumis* 

Depto. de Sistemas Complejos, Instituto de Física, Universidad Nacional Autónoma de México (UNAM),
Apdo. Postal 20-364, 01000 CDMX, Mexico

E-mail: naumis@fisica.unam.mx

Received 12 June 2023, revised 12 September 2023

Accepted for publication 20 September 2023

Published 28 September 2023



CrossMark

Abstract

The topological properties of the flat band states of a one-electron Hamiltonian that describes a chain of atoms with $s - p$ orbitals are explored. This model is mapped onto a Kitaev–Creutz type model, providing a useful framework to understand the topology through a nontrivial winding number and the geometry introduced by the *Fubini–Study (FS)* metric. This metric allows us to distinguish between pure states of systems with the same topology and thus provides a suitable tool for obtaining the fingerprint of flat bands. Moreover, it provides an appealing geometrical picture for describing flat bands as it can be associated with a local conformal transformation over circles in a complex plane. In addition, the presented model allows us to relate the topology with the formation of compact localized states and pseudo-Bogoliubov modes. Also, the properties of the squared Hamiltonian are investigated in order to provide a better understanding of the localization properties and the spectrum. The presented model is equivalent to two coupled SSH chains under a change of basis.

Keywords: flat bands, winding number, Fubini–Study metric, Kitaev–Creutz model

1. Introduction

A flat band (FB) refers to a band with constant energy unaffected by the crystal momentum. This property suppresses wave transport and makes it highly sensitive to perturbations [1]. This has led to the exploration of partially FBs, which have

vanishing dispersion along specific directions or near particular points in the Brillouin zone [2–4].

Due to their unique characteristics, FB systems have been a subject of great interest in several research fields [5–12], such as the generation of electronic correlations in condensed matter [13–18]; among such phenomena include ferromagnetism [13, 14], superconductivity [15, 16], and Wigner crystal formation [17, 18], and in photonics leading to slow-light realizations [19, 20] and coherent propagation free of quantum dispersion [21, 22]. Thus, the study of FB systems is crucial because it provides insight into the collective phenomena that govern the behavior of complex materials [13, 23–26]. These materials are of great interest because they have

* Author to whom any correspondence should be addressed.



Original Content from this work may be used under the terms of the [Creative Commons Attribution 4.0 licence](https://creativecommons.org/licenses/by/4.0/). Any further distribution of this work must maintain attribution to the author(s) and the title of the work, journal citation and DOI.

the potential to revolutionize many areas, such as electronics and possible applications to quantum computing [27].

Historically, developing FB models has been a long and arduous process. It started with Sutherland's discovery of a FB in the dice lattice [28]. It continued with Lieb's work on the Hubbard model, demonstrating that certain bipartite lattices with chiral FBs exhibit ferromagnetism [29]. However, in recent years, there has been a growing interest in the development of new topological FB models [2] that will allow for a better understanding of the properties of these materials and their potential applications and which can support quantum Hall (QH)-like states, including integer QH effect [30, 31], fractional QH (FQH) effect [32–34], and the existence of electronic fractional Chern states [11, 12, 32, 35].

Lastly, one of the challenges in studying FB systems is distinguishing between pure states of systems with the same topology. To overcome this challenge, in previous work, the FS metric has been introduced as a tool, mainly to differentiate quantum states in FBs [36–39]. This metric enables the reliable identification of flatness regions in topological systems.

This paper presents a non-superconducting one-dimensional tight-binding model that can be mapped to a Kitaev chain Hamiltonian, preserving its topological properties with a nontrivial winding number. The FS metric of the model allows for the construction of a mapping f that can accurately distinguish between topological and nontopological systems, as well as between topological systems with and without FBs. This model is inspired by recent experimental evidence of one-dimensional FBs along established directions in two-dimensional van der Waals structures [40], as well as research that suggests that chains of elements such as boron [41], gallium [42] and tellurium [43, 44] could be used to realize the proposed model experimentally.

This paper is organized as follows. Section 2 introduces the atomic chain model and the effective Hamiltonian. Section 3 discusses the formation of pseudo-Bogoliubov modes and a regime with FBs where compact localized states (CLS) exist. These bands are characterized by relations similar to those found in Landau levels. Additionally, we demonstrate a nontrivial topology phase transition and how the geometry described by the FS metric enables the mapping f to be constructed to differentiate between FB regimes and other topological systems. Finally, section 4 summarizes our findings.

2. Model and methods

As explained in the introduction, our main motivation here is to find a model with realistic features such that it contains a FB susceptible of being treated analytically in a simple way. FBs are associated with zero group velocity and this requires destructive wave interference. Clearly, a model based only on pure s orbitals is not able to produce such effect. The change of sign induced by p orbitals when rotated by an angle of π induces such possibility as positive and negative interactions of the same magnitude appear. Therefore, the most simple model is to have a one-dimensional system with $s-p$ orbitals (see figure 1(a)). Notice that here we do not introduce p_y

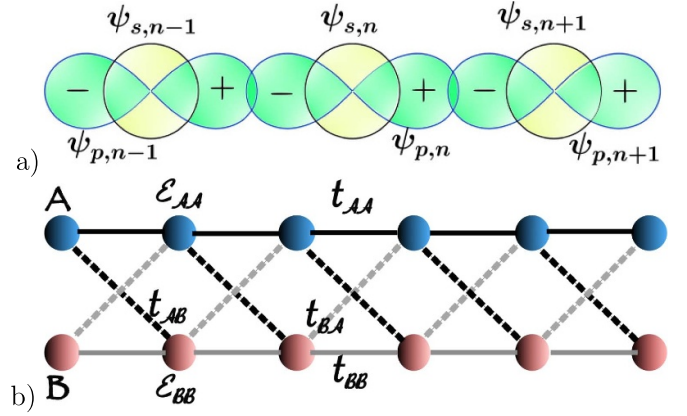


Figure 1. (a) At each site of the atomic chain, there are two orbitals s and p_x , denoted as $\psi_{s,n}$ and $\psi_{p,n}$. The hopping integrals of the nearest-neighbor t_{pp} and t_{ss} have the opposite sign, while the nearest-neighbor t_{sp} couplings alternate in sign. Due to inversion symmetry, the on-site t_{sp} coupling will be zero, just like in an isolated atom. The tight-binding Hamiltonian is given by equation (1). (b) This atomic chain can be geometrically represented as an unbalanced Creutz ladder [10, 45–48], where the blue and red circles represent the sites A and B , respectively. The orbitals s and p correspond to the sites A and B , and the hoppings follow the rules $t_{ss} \rightarrow t_{AA}$ (black lines), $t_{pp} \rightarrow t_{BB}$ (gray lines), $t_{sp(ps)} \rightarrow t_{AB(BA)}$ (dashed black (gray) lines) and $\varepsilon_{s(p)} \rightarrow \varepsilon_{A(B)}$ (see equation (2)).

and p_z orbitals due to several reasons. The first is that we want to keep the model simple to shine light in the Fubini–Study metric topological study. But there are other physical reasons to proceed in such a way. One is that such simple system can be implemented using quantum analogous systems like in ultracold atom lattices [45] or simulate topological zero modes (flat bands) on a qubit superconducting processor [49]. Having only one type of p orbitals simplify considerably the complexity of the device. The second reason is that chalcogenide elements as Se or Te form chains [44]. The bonds are directed along the chain direction and thus are well described with only one type of p orbitals.

Under such considerations, our investigation is based on a tight-binding model with only first-neighbors hopping, which yields a Hamiltonian that can be expressed as

$$\hat{\mathcal{H}} = \sum_{\mathbf{r}_n} (\varepsilon_s(\mathbf{r}_n) c_{s,\mathbf{r}_n}^\dagger c_{s,\mathbf{r}_n} + \varepsilon_p(\mathbf{r}_n) c_{p,\mathbf{r}_n}^\dagger c_{p,\mathbf{r}_n}) + \sum_{\mathbf{r}_n} \left[t_{ss}(\mathbf{r}_n) c_{s,\mathbf{r}_{n+1}}^\dagger c_{s,\mathbf{r}_n} + t_{pp}(\mathbf{r}_n) c_{p,\mathbf{r}_{n+1}}^\dagger c_{p,\mathbf{r}_n} + t_{sp}(\mathbf{r}_n) c_{p,\mathbf{r}_{n+1}}^\dagger c_{s,\mathbf{r}_n} + t_{ps}(\mathbf{r}_n) c_{s,\mathbf{r}_{n+1}}^\dagger c_{p,\mathbf{r}_n} \right] + h.c. \quad (1)$$

The indices s and p refer to the respective orbitals, and \mathbf{r}_n is the position of the n -th atom. The fermionic annihilation (creation) operator for orbital s and p is denoted by $c_{(s,p),\mathbf{r}_n}$ ($c_{(s,p),\mathbf{r}_n}^\dagger$), while $\varepsilon_{(s,p)}(\mathbf{r}_n)$ and $t_{ss}(\mathbf{r}_n), t_{pp}(\mathbf{r}_n), t_{sp}(\mathbf{r}_n), t_{ps}(\mathbf{r}_n)$ are the energy on-site and the hopping parameter to the first right neighbor, respectively. Assuming that $\varepsilon_\alpha(\mathbf{r}_n)$ and $t_{\alpha,\beta}(\mathbf{r}_n)$ are independent of the atomic position, the tight-binding parameters $t_{ss}, t_{pp}, t_{sp}, t_{ps}$ can be obtained.

We can think of the chain as a ladder, with each s and p orbital mapped to different sites. As illustrated in figure 1(b), the ladder consists of two types of sites: type A, which is derived from the s orbitals and type B, which is derived from the p orbitals. This ladder is equivalent to a Creutz model, and its Hamiltonian is given by

$$\mathcal{H} = \sum_n (\varepsilon_A a_n^\dagger a_n + \varepsilon_B b_n^\dagger b_n) + \sum_n (t_{AA} a_{n+1}^\dagger a_n + t_{BB} b_{n+1}^\dagger b_n + t_{AB} b_{n+1}^\dagger a_n + t_{BA} a_{n+1}^\dagger b_n) + h.c. \quad (2)$$

The annihilation (creation) operators for sites A and B in the cell n are indicated by a_n (a_n^\dagger) and b_n (b_n^\dagger), respectively. It has been demonstrated that due to the symmetry of the p orbitals, $t_{ps} = -t_{sp}$ and $t_{pp} = -t_{ss}$ [50]; consequently $t_{AA} = -t_{BB}$ and $t_{AB} = -t_{BA}$. In addition to this, we assume that $\varepsilon_{AA} = -\varepsilon_{BB}$, then the Hamiltonian is given by

$$\mathcal{H} = \varepsilon \sum_n (a_n^\dagger a_n - b_n^\dagger b_n) + \sum_n t_{AA} (a_{n+1}^\dagger a_n - b_{n+1}^\dagger b_n) + t_{AB} (b_{n+1}^\dagger a_n - a_{n+1}^\dagger b_n) + h.c. \quad (3)$$

We then perform a lattice Fourier transformation using the operators

$$a_k = \frac{1}{\sqrt{N}} \sum_n a_n e^{ikx_n} \text{ and } b_k = \frac{1}{\sqrt{N}} \sum_n b_n e^{ikx_n}, \quad (4)$$

where $x_n = nl$ and l is the lattice constant. Finally, this allows us to rewrite the Hamiltonian equation (3) in the standard Bogoliubov–de Gennes form.

$$\mathcal{H} = t_{AA} \sum_k \Psi_k^\dagger \mathcal{H}(k) \Psi_k, \quad \Psi_k = (a_k, b_k)^T. \quad (5)$$

where,

$$\mathcal{H}(k) = \mathbf{n}(k) \cdot \boldsymbol{\sigma} = n_x(k) \sigma_x + n_y(k) \sigma_y + n_z(k) \sigma_z \quad (6)$$

and the coefficients that accompany the Pauli matrices $\sigma_x, \sigma_y, \sigma_z$ are $n_x(k) = 0, n_y(k) = 2\lambda \sin(kl), n_z(k) = (\bar{\varepsilon} + 2\cos(kl))$. Here, $\bar{\varepsilon}$ and λ are dimensionless parameters that capture the information of the parameters ε and t_{AB} of the Hamiltonian (3), respectively, and are defined as $\bar{\varepsilon} \equiv \varepsilon/t_{AA}$ and $\lambda \equiv t_{AB}/t_{AA}$.

3. Results

In this section, we explore the properties of the model proposed in equation (5). We examine the emergence of Bogoliubov and Majorana pseudo modes, their equivalence with the Kitaev Hamiltonian, their topological properties demonstrated by a nontrivial winding number, and the presence of a regime with topological FBs and similarities to Landau levels. Additionally, we show that this system is equivalent to two coupled SSH chains and two decoupled chains with the next-nearest neighbor hopping, and we introduce a conformal transformation that allows us to identify topological and nontopological regimes and between flat and dispersive bands.

3.1. Pseudo-Bogoliubov and Majorana modes

We can define two pseudo-Bogoliubov modes, γ_k and ρ_k , using the Hamiltonian in equation (5). These modes are a combination of a fermion at sites A and B and are analogous to the Bogoliubov quasiparticles. They are expressed as

$$\gamma_k \equiv u_k a_k + v_k b_k, \quad \rho_k \equiv -v_k^* a_k + u_k^* b_k, \quad (7)$$

where u_k and v_k are the coefficients that define the Bogoliubov modes. These pseudo-Bogoliubov modes hybridize orbitals s and p , and satisfy the fermionic creation and annihilation anti-commutation relations (see appendix).

$$\begin{aligned} \{\rho_k, \rho_{k'}^\dagger\} &= \delta_{kk'}; \quad \{\rho_k^\dagger, \rho_{k'}^\dagger\} = \{\rho_k, \rho_{k'}\} = 0; \\ \{\gamma_k, \gamma_{k'}^\dagger\} &= \delta_{kk'}; \quad \{\gamma_k^\dagger, \gamma_{k'}^\dagger\} = \{\gamma_k, \gamma_{k'}\} = 0 \end{aligned} \quad (8)$$

where u_k and v_k must meet the criteria of $u_k^2 + v_k^2 = 1, u_{-k} = u_k$ and $v_{-k} = -v_k$. A suitable selection of u_k and v_k will satisfy these conditions.

$$u_k = \cos\left(\frac{\omega_k}{2}\right), \quad v_k = -i \sin\left(\frac{\omega_k}{2}\right), \quad (9)$$

where we defined,

$$\omega_k = \text{Arg}\{2i\lambda \sin(kl) + (\bar{\varepsilon} + 2\cos(kl))\}. \quad (10)$$

Here, $\text{Arg}(z)$ refers to the principal value of $z \in \mathbb{C}$. When substituting a_k, b_k into equation (5), we diagonalize the Hamiltonian to obtain

$$\begin{aligned} \mathcal{H} &= t_{AA} \sum_k \epsilon(k) \left(\gamma_k^\dagger \gamma_k - \rho_k^\dagger \rho_k \right) \text{ with} \\ \epsilon(k) &= \sqrt{(\bar{\varepsilon} + 2\cos(kl))^2 + (2\lambda \sin(kl))^2}. \end{aligned} \quad (11)$$

Generally, these pseudo-Bogoliubov modes are associated with squeezed coherent states [51] and, in a similar form, have recently been observed in twisted bilayer graphene (TBLG) at magic angles [52].

In the long-wavelength limit, we can expand the Hamiltonian (5) at $k=0$ to obtain

$$\begin{aligned} \mathcal{H} &= t_{AA} \sum_k \Psi_k^\dagger H_D(k) \Psi_k \text{ with } H_D(k) = m\sigma_z + 2\lambda kl\sigma_y \text{ and} \\ m &= (\bar{\varepsilon} - \bar{\varepsilon}_c). \end{aligned} \quad (12)$$

where $\bar{\varepsilon}_c = -2$ and the energy dispersion is given by $\epsilon(k) = \pm \sqrt{(\bar{\varepsilon} - \bar{\varepsilon}_c)^2 + 4\lambda^2 k^2 l^2}$. As shown in figure 2, there is an energy gap of size $\Delta = 2(\bar{\varepsilon} - \bar{\varepsilon}_c)$ that vanishes when the critical value $\bar{\varepsilon}_c$ is reached, that is, when m is close to zero. At this point, the energy dispersion follows the relation $\epsilon(k) = \pm 2\lambda lk$, implying that the pseudo-Bogoliubov modes can be interpreted as pseudo-Majorana modes, and they can move along the chain with a velocity of $v = 2\lambda l$. As the mass approaches zero, the energy of these eigenstates is equal.

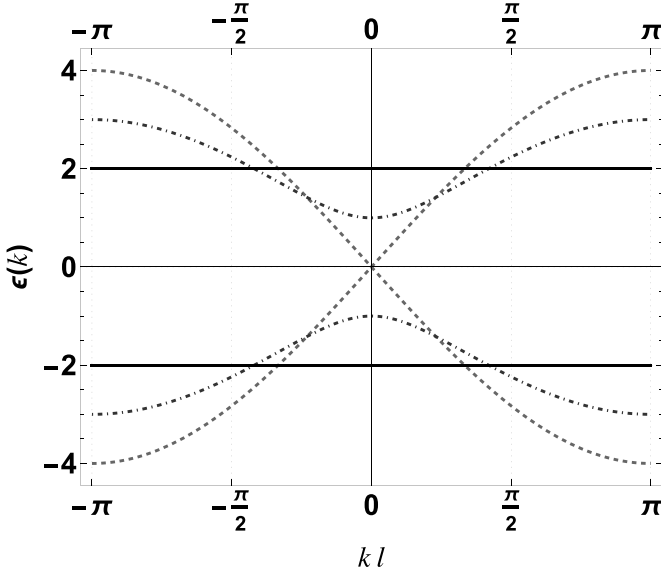


Figure 2. The band structure of the Kitaev–Creutz ladder model as a function of kl , and for the set of values $\lambda = 1$, $l = 1$, and $\bar{\epsilon} = -2$ (dotted line), $\bar{\epsilon} = -1$ (dot-dashed line), and $\bar{\epsilon} = 0$ (solid line), respectively (see equation (11)).

3.2. Topological properties I: nontrivial winding number

The Hamiltonian (5) can be exactly mapped to a Kitaev Hamiltonian, extensively studied by Leumer *et al* [53]. Hence, our model is referred to as the Kitaev–Creutz model and the correspondence is as follows

$$\bar{\epsilon} \rightarrow -\mu/t, \quad \lambda \rightarrow -\Delta/t, \quad (13)$$

however, the physics interpretation is not the same. It has been demonstrated in [53] that the Hamiltonian (5) is invariant under time-reversal symmetry for spinless fermions $\mathcal{T} = \mathbb{1}\mathcal{K}$, with \mathcal{K} being the complex conjugation and the chiral symmetry $\mathcal{TP} = \mathcal{C} = \sigma_x$. Additionally, it anti-commutes with the particle-hole operator $\mathcal{P} = \sigma_x\mathcal{K}$. Therefore, the particle-hole symmetry establishes that the band structure is symmetric with respect to the zero energy. Note that the Kitaev Hamiltonian belongs to the BDI class [54], where all square symmetries operators are the identity.

The chiral symmetry allows us to define the winding number as the topological invariant [55], where the winding number is defined as [55, 56]

$$\nu = \frac{1}{2\pi} \int_{-\pi/l}^{\pi/l} dk \partial_k \omega_k, \quad (14)$$

here $\partial_k \omega_k$ is the winding number density [53, 55]. The phase diagram in figure 3 is similar to that of a Kitaev chain with the appropriate parameters [53]. The dashed black lines in figure 3 a) indicate the boundaries between the topological phases with $\bar{\epsilon} = \pm 2$, which meet the condition $\epsilon(k) = 0$ in $kl = 0, \pm\pi d$ and $\lambda \neq 0$. Figures 3 (b) and (c) show the curves of parameterization $(n_y(k), n_z(k))$ (cf equation (5)) along the Brillouin zone (BZ) with different values of $\bar{\epsilon}$ and λ , with the winding number being the topological invariant.

3.3. FBs, CLS and analogous Landau levels relations

When a FB is present, the group velocity of the charge carriers is zero for all momenta in the Brillouin zone, indicating that the charge carriers are localized. This localization is caused by the presence of a particular localized eigenstate, known as the CLS. This state has a finite amplitude within a finite region in real space and is zero outside. It should be noted that CLS is not unique and can be of multiple types, depending on the linear combinations of the smallest CLSs centered at different positions [57].

The eigenvalues of the Hamiltonian, as demonstrated by equation (5), have two topological FBs with $\epsilon(k) = \pm 2$ when $\bar{\epsilon} = 0$ and $\lambda = \pm 1$, in this regime $\nu = \mp 1$ (see figure 3). Furthermore, the electrons can obtain a phase difference of π along closed trajectories (see figure 4(a)). The Bloch state creation operator for the FB is expressed as

$$\Psi_{k,\lambda,\pm}^\dagger = \frac{1}{2} \left\{ \left(e^{i\lambda kl/2} \pm e^{-i\lambda kl/2} \right) a_k^\dagger + \left(e^{i\lambda kl/2} \mp e^{-i\lambda kl/2} \right) b_k^\dagger \right\} \quad (15)$$

where the sign \pm is for $\epsilon(k) = \pm 2$, respectively.

The energy degeneracy means that any combination of the FB Bloch states is an eigenstate. Furthermore, the Fourier transform of these states is also an eigenstate. To illustrate this, let us calculate the Fourier transform of equation (15).

$$\Psi_{y_n,\lambda,\pm}^\dagger = \mathcal{N} \int_{\text{BZ}} dk e^{iky_n} \Psi_{k,\lambda,\pm}^\dagger = \frac{1}{2} \left(a_n^\dagger \pm a_{n-\lambda}^\dagger + b_n^\dagger \mp b_{n-\lambda}^\dagger \right) \quad (16)$$

where $y_n = x_n - l/2$ and \mathcal{N} is a normalization constant. As shown in figure 4(b), $\Psi_{y_n,\lambda,\pm}$ takes the form of a localized square plaquette centered y_n , that is, between cell n and $n - 1$.

One can verify that the sites of plaquettes obey the following relations, analogous to Landau levels states relations [30],

$$\begin{aligned} \sum_{y_n} (-1)^n \Psi_{y_n,\lambda,+}^{(1)} + \Psi_{y_n,\lambda,+}^{(2)} &= 0 \text{ and} \\ \sum_{y_n} \Psi_{y_n,\lambda,-}^{(1)} + (-1)^n \Psi_{y_n,\lambda,-}^{(2)} &= 0 \end{aligned} \quad (17)$$

with $\Psi^{(1,2)}$ as the first- and second- component of the FB Bloch state. A recent study [58] has also demonstrated a connection between FBs and Landau levels. Due to destructive interference, the electron is confined within the plaquette, resulting in a quenched kinetic energy that FB regulates.

Let us now write a Bloch state as

$$|u_k^\pm\rangle = \frac{1}{2} \left(e^{i\omega_k/2} \pm e^{-i\omega_k/2}, e^{i\omega_k/2} \mp e^{-i\omega_k/2} \right)^T. \quad (18)$$

Therefore, the eigenstates in the real space are

$$|\psi_\pm(x)\rangle = \frac{l}{2\pi} \int_{-\pi/l}^{\pi/l} dk e^{ikx} |u_k^\pm\rangle \equiv (\psi_{A,\pm}(x), \psi_{B,\pm}(x))^T \quad (19)$$

Figure 5 shows the eigenfunction in real space for sites A and B with different values of $\bar{\epsilon}$, keeping $\lambda = 1$. As can be

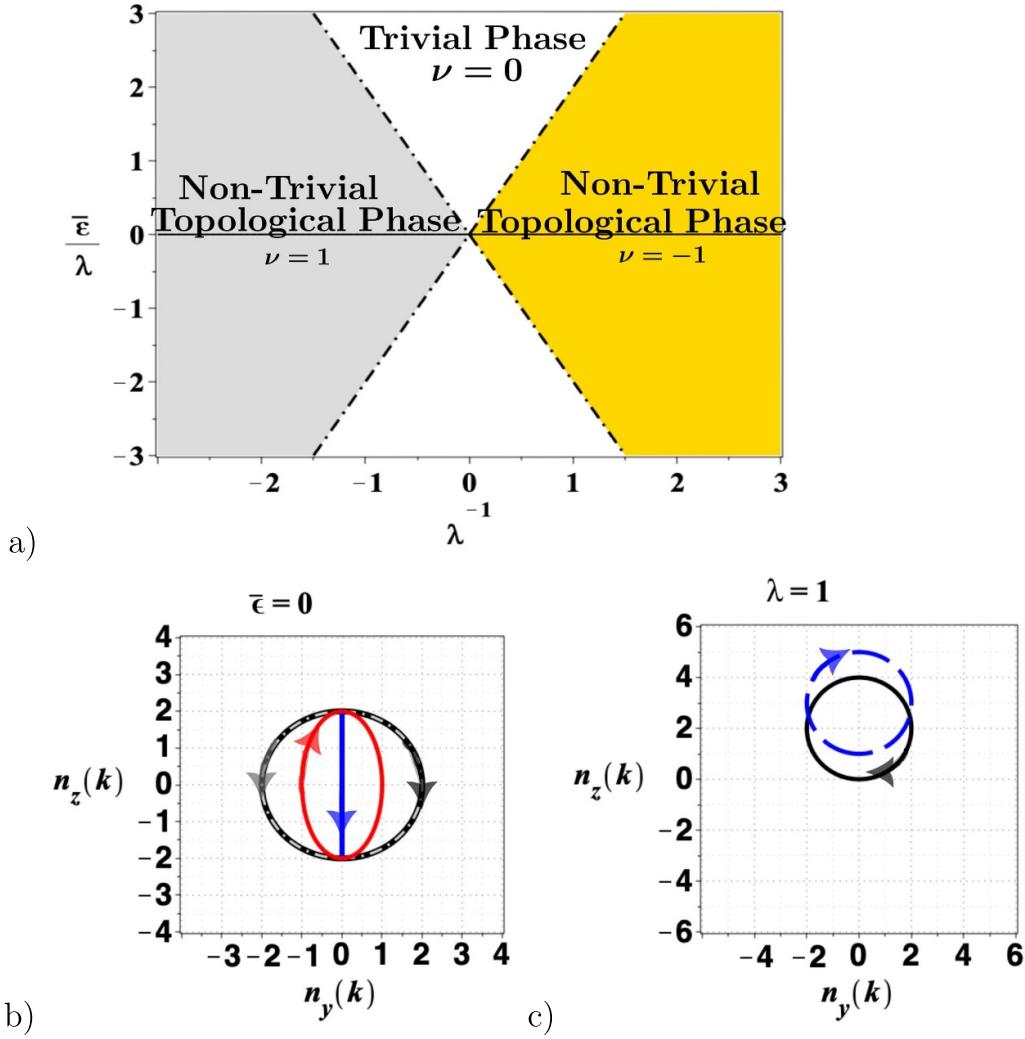


Figure 3. The topological phase diagram of the Kitaev–Creutz ladder system with Hamiltonian (5) is shown in figure (a) using equation (14). The dashed black lines indicate the boundaries between the topological phases, which are determined by the condition $\bar{\epsilon} = \pm 2$. The curves in panels (b) and (c) correspond to the parameterization $(n_y(k), n_z(k))$ (cf equation (5)), where $k \in \text{BZ}$. In figure (b), the curves for $\lambda = -1$ (gray circle), $\lambda = 0$ (blue line), $\lambda = 1/2$ (red ellipse), and $\lambda = 1$ (black circle) are plotted with $\bar{\epsilon} = 0$. In figure (c), the curves for $\bar{\epsilon} = 2$ (black circle) and $\bar{\epsilon} = 3$ (blue dashed circle) are plotted with $\lambda = 1$. It is noteworthy that for the blue line in figure (b) and the black circle in figure (c), the winding number is not well defined since the curve passes through the origin.

seen in figure 5(a) and (b), there is constructive and destructive interference between sites A and B , respectively. This is contrary to what is observed in figure 5(c) and (d). This is in accordance with equation (16) due to the change of sign when considering a conduction and valence bands. Furthermore, when $\bar{\epsilon} = 0$, the electron density for the sites A and B is sharper than in any other of the scenarios; however, in this case, the spectrum is also highly degenerate so as explained in section 3.5, care must be taken in its interpretation.

3.4. Equivalent SSH model

We can observe a periodic chain with a two-sublattice structure in figure 1(b). Sites on sublattice A have the diagonal hopping to the left, t_{AB} , and right t_{BA} , while for sites belonging to the other sublattice, it is just the opposite. According to the assumptions in equation (3), the time-independent Schrödinger equation can be transformed into equivalent

difference equation forms for any pair of sites. Therefore, the following pairs of equations are valid for the given system.

$$\begin{aligned} (E - \varepsilon) \psi_{A,n} &= t_{AA} (\psi_{A,n-1} + \psi_{A,n+1}) + t_{AB} (\psi_{B,n+1} - \psi_{B,n-1}) \\ (E + \varepsilon) \psi_{B,n} &= -t_{AA} (\psi_{B,n+1} + \psi_{B,n-1}) + t_{AB} (\psi_{A,n-1} - \psi_{A,n+1}). \end{aligned} \quad (20)$$

To facilitate the analysis, we introduce the following basis transformation

$$\begin{pmatrix} \phi_{1,n} \\ \phi_{2,n} \end{pmatrix} = M \begin{pmatrix} \psi_{A,n} \\ \psi_{B,n} \end{pmatrix}, \quad M = \begin{pmatrix} 1 & 1 \\ 1 & -1 \end{pmatrix}. \quad (21)$$

Then, from equations (20) and (21), we obtain the following equations

$$\begin{aligned} \bar{E} \phi_{1,n} - \bar{\varepsilon} \phi_{2,n} &= (1 - \lambda) \phi_{2,n+1} + (1 + \lambda) \phi_{2,n-1} \\ \bar{E} \phi_{2,n} - \bar{\varepsilon} \phi_{1,n} &= (1 + \lambda) \phi_{1,n+1} + (1 - \lambda) \phi_{1,n-1} \end{aligned} \quad (22)$$

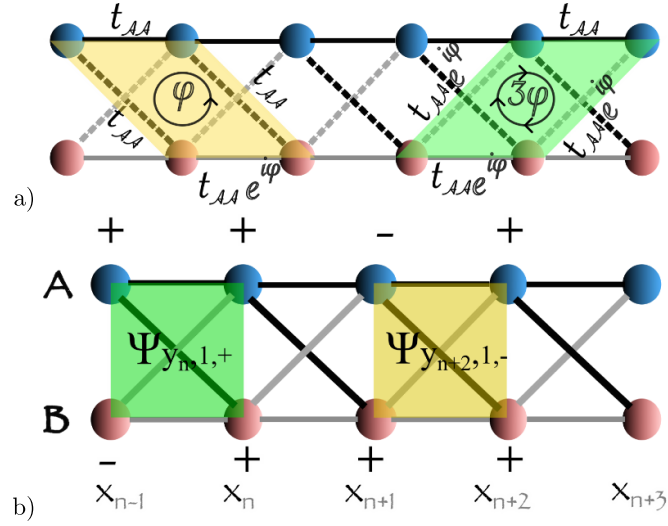


Figure 4. (a) In this flat band regime, we observe that when two different closed paths are followed, the fermions acquire a phase difference of ϕ and 3ϕ with $\phi = \pi$, resulting in a π -flux in the Kitaev–Creutz type ladder model in equation (5). (b) The two CSLs in the flat band regime are represented by filled regions, with the signs of their component amplitudes indicated (see equation (16)).

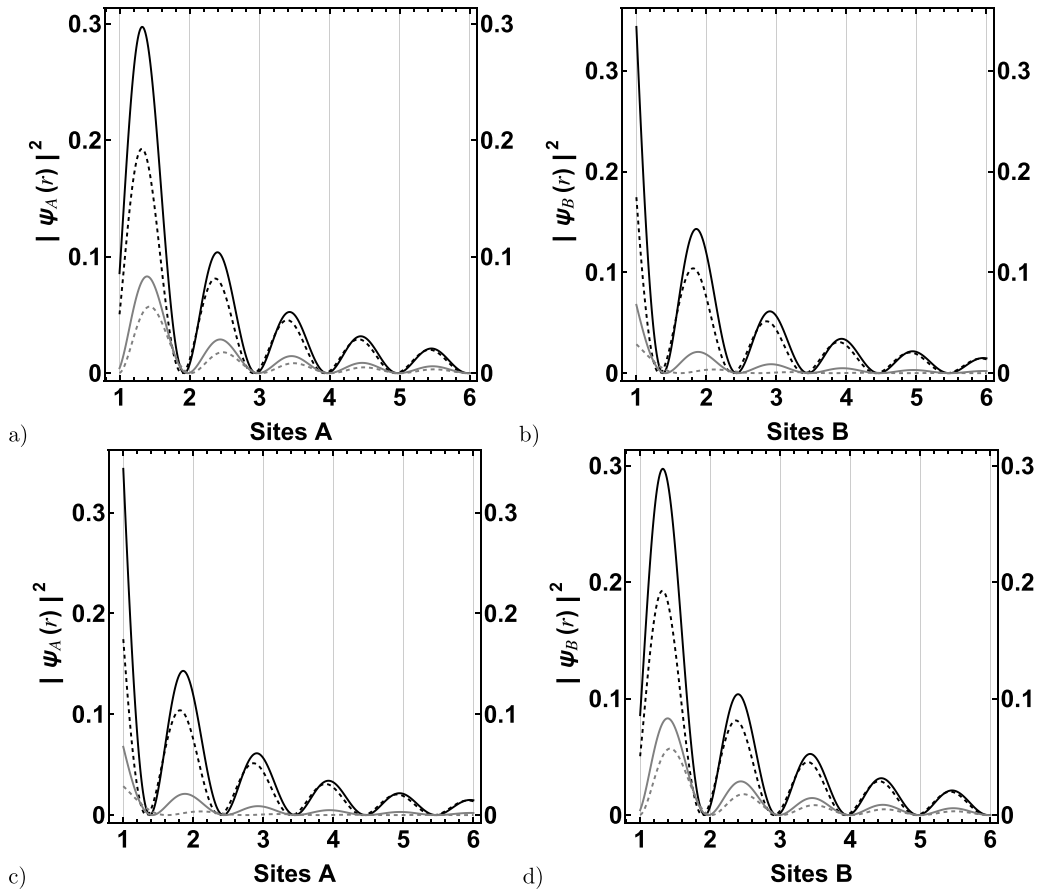


Figure 5. The electron density for sites *A* and *B* is shown in panels (a), (b) for the conduction band and in panels (c), (d) for the valence band. The used parameters were $\lambda = 1$ and $\bar{\epsilon} = 0$ (solid black curve), $\bar{\epsilon} = 1$ (dashed black curve), $\bar{\epsilon} = 2$ (solid gray curve) and $\bar{\epsilon} = 3$ (gray dots). In analogy to equation (16), at sites *A* and *B* there is constructive and destructive interference in the conduction band case and vice versa in the valence band case. Notice how as the system approaches the flat band case ($\bar{\epsilon} = 0$) the peaks tend to be more pronounced.

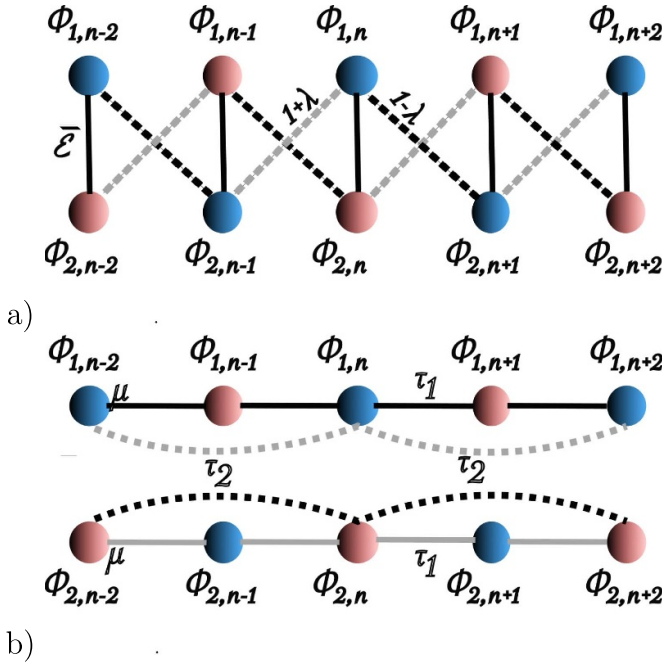


Figure 6. (a) By transforming the basis (equation (22)) of the Kitaev–Creutz model, we obtain an equivalent ladder consisting of two SSH chains that are distinguished by red and blue sites (see the online version). (b) This equivalent ladder can be divided into two chains with hopping of the first and second neighbors in equation (23). Isolated atomic-like states, or CLS, are obtained at each site when $\lambda \rightarrow \pm 1$ and $\bar{\epsilon} = 0$ with $\tau_1 = \tau_2 = 0$.

where $\bar{E} = E/t_{AA}$. This equation system corresponds to two coupled SSH chains, as depicted in figure 6(a).

3.5. Supersymmetric transformation by squaring the Hamiltonian

In this subsection we will show that the square of the Hamiltonian decouples the sublattices and renormalizes the hopping and on-site energies making it somewhat analogous to a phonon problem and akin to a supersymmetric transformation [59–62]. To understand this, from equation (22), we use the second equation in the first and vice versa. Then equation (22) can be rewritten as

$$\begin{aligned} (\bar{E}^2 - \mu) \phi_{j,n} &= \tau_1 (\phi_{j,n-1} + \phi_{j,n+1}) \\ &+ \tau_2 (\phi_{j,n+2} + \phi_{j,n-2}), j = 1, 2. \end{aligned} \quad (23)$$

with $\mu = \bar{\epsilon}^2 + 2(1 + \lambda^2)$, $\tau_1 = 2\bar{\epsilon}$, and $\tau_2 = (1 - \lambda^2)$.

Equation (23) is equivalent to square the Hamiltonian (3). It is also equivalent to remove one of the bipartite sublattices [11, 63, 64], in this case for the Kitaev–Creutz ladder leaving two decoupled periodic chains with nearest neighbor hoppings (τ_1), next-nearest hoppings (τ_2) and with an effective on-site energy μ (see figure 6(b)). The dispersion relations are obtained from equation (23) using a procedure similar to that exposed in equation (11),

$$\begin{aligned} \bar{E}^2 &= \mu + 2\tau_1 \cos(kl) + 2\tau_2 \cos(2kl) \\ \Leftrightarrow \bar{E}_{\pm} &= \pm \sqrt{(\bar{\epsilon} + 2 \cos(kl))^2 + 4\lambda^2 \sin^2(kl)} \end{aligned} \quad (24)$$

or in a simpler form, by taking the square of the Hamiltonian (6) which reduces to

$$\mathcal{H}^2(k) = \begin{pmatrix} \epsilon^2(k) & 0 \\ 0 & \epsilon^2(k) \end{pmatrix} \quad (25)$$

The eigenvalues of $\mathcal{H}^2(k)$ are simply the square of those of $\mathcal{H}(k)$ explaining the hole-particle symmetry of the spectrum seen in figure 2. We now observe that while any eigenfunction of $\mathcal{H}(k)$ is also an eigenfunction of $\mathcal{H}^2(k)$, the inverse is not necessarily true. Thus, the eigenfunctions of $\mathcal{H}(k)$ are sublattice polarized while those of $\mathcal{H}^2(k)$ are not necessarily polarized.

In the FB regime ($\bar{\epsilon} = 0, |\lambda| = 1$), and from equation (23), $\tau_1 = \tau_2 = 0$ indicating the existence of localized atomic-like states that are equivalent to the CLS shown in section 3.3 (see figure 6(b)). Moreover, for the FB $\mathcal{H}^2(k) = (4) \mathbb{1}_{2 \times 2}$ and the eigenfunctions are arbitrary linear combinations of the basis vectors $(1, 0)^T$ and $(0, 1)^T$. This emphasizes the very peculiar localization properties of FBs as seen in other systems [12, 58, 64]. Therefore, the FB now becomes a massive degenerate ground state of $\mathcal{H}^2(k)$. As in other systems, the squared Hamiltonian can be interpreted as a massive vibrational band [11] quite similar to the protected electronic boundary modes found in the QHE and topological insulators [65] and which are well-known in the rigidity theory of glasses [66–68].

3.6. Topological properties II: Fubini–Study metric

The quantum geometry tensor is a key factor in understanding the behavior and characteristics of physical systems at the quantum level. It is particularly useful in the analysis of topological insulators and materials with FBs. Moreover, it can be used to gain insight into the electronic structure and properties of these materials [36–39].

In general, we consider a quantum state $|\psi(\xi)\rangle$ in the N -dimensional parameter space, where $\xi = (\xi_1, \xi_2, \dots, \xi_N)$ is a set of parameters. Thus, this space can be endowed with the geometric quantum tensor [69–74], given by

$$Q_{\mu\nu}(\xi) \equiv \langle \partial_\mu \psi(\xi) | \mathbb{P}_{\psi(\xi)} | \partial_\nu \psi(\xi) \rangle \quad (26)$$

where $\mathbb{P}_{\psi(\xi)}$ is the orthogonal complement projector,

$$\mathbb{P}_{\psi(\xi)} = \mathbb{1} - |\psi(\xi)\rangle \langle \psi(\xi)|. \quad (27)$$

Since $Q_{\mu\nu}$ can have complex values, this leads to the *FS* metric ($g_{\mu\nu}$), which is the real part of the quantum metric $g_{\mu\nu}(\xi) = \text{Re}[Q_{\mu\nu}(\xi)]$. The imaginary part is associated with the Berry curvature $\Omega_{\mu\nu}(\xi)$ and is given by

$$\text{Im}[Q_{\mu\nu}] = -\frac{\Omega_{\mu\nu}}{2}. \quad (28)$$

The *FS* metric measures the statistical distance between nearby pure quantum states $|\psi(\xi)\rangle$ and $|\psi(\xi + d\xi)\rangle$, providing a means of distinguishing them [75].

For calculating the *FS* metric, it is necessary to consider the Bloch states, which are given by

$$\begin{aligned} |u_k^+\rangle &= (\cos(\omega_k/2), i \sin(\omega_k/2))^T, \text{ for conduction band} \\ |u_k^-\rangle &= (i \sin(\omega_k/2), \cos(\omega_k/2))^T, \text{ for valence band.} \end{aligned} \quad (29)$$

Then, the derivatives are

$$|\partial_k u_k^+\rangle = \frac{\partial_k \omega_k}{2} (-\sin(\omega_k/2), i \cos(\omega_k/2))^T, \quad (30)$$

$$|\partial_k u_k^-\rangle = \frac{\partial_k \omega_k}{2} (i \cos(\omega_k/2), -\sin(\omega_k/2))^T. \quad (31)$$

and following the formula for the *FS* metric, it can be proved that [75, 76]

$$g_{kk}^\pm = \langle \partial_k u_k^\pm | \partial_k u_k^\pm \rangle - \langle \partial_k u_k^\pm | u_k^\pm \rangle \langle u_k^\pm | \partial_k u_k^\pm \rangle = \left(\frac{\partial_k \omega_k}{2} \right)^2. \quad (32)$$

The first observation is that from equation (32) it follows

$$\sqrt{\det(g_{kk}^\pm)} = \frac{|\partial_k \omega_k|}{2}. \quad (33)$$

We define the quantities $\text{vol}(\text{BZ})$ and $\text{vol}(S^1)$ given by

$$\text{vol}(\text{BZ}) \equiv \int_{\text{BZ}} \sqrt{\det(g_{kk}^\pm)} dk, \quad \text{Vol}(S^1) \equiv \int_{S^1} d\theta. \quad (34)$$

In the case where the *FS* metric are nondegenerate, $\text{vol}(\text{BZ})$ and $\text{vol}(S^1)$ correspond to the *volumes* of the Brillouin Zone (BZ) and the unitary circle S^1 , respectively. Thus, we obtained from equations (14), (33), (34) the following inequalities

$$\pi |\nu| \leq \text{vol}(\text{BZ}) \leq \frac{1}{2} \text{vol}(S^1). \quad (35)$$

Therefore, the minimum value of the quantum volume is determined by the winding number of the occupied Bloch bundle. In the 2D case, this is equivalent to the result found by Ozawa and Mera, where the equalities are associated with a flat Kähler structure [37–39, 77]. This 2D version has also been used in topological superconductors to establish a relationship between the topological properties of the system and the superfluid weight, as demonstrated in [78–83].

On the other hand, to understand the geometry related to the *FS* metric tensor, g_{kk}^\pm , it is necessary to consider the *FS* arc element ds_{FS} and the usual infinitesimal line elements in S^1 , ds_{S^1} , which are given by

$$ds_{FS}^2 = g_{kk}^\pm dk^2 = \left(\frac{1}{2} \right)^2 d\omega_k^2, \quad |k| \leq \pi/l \text{ and } ds_{S^1}^2 = d\theta^2, \quad |\theta| \leq \pi. \quad (36)$$

Thus, from equation (36), we show that there is a locally conformal transformation between S^1 and the *FS* manifold. Furthermore, we can conceive the space *FS* and S^1 as

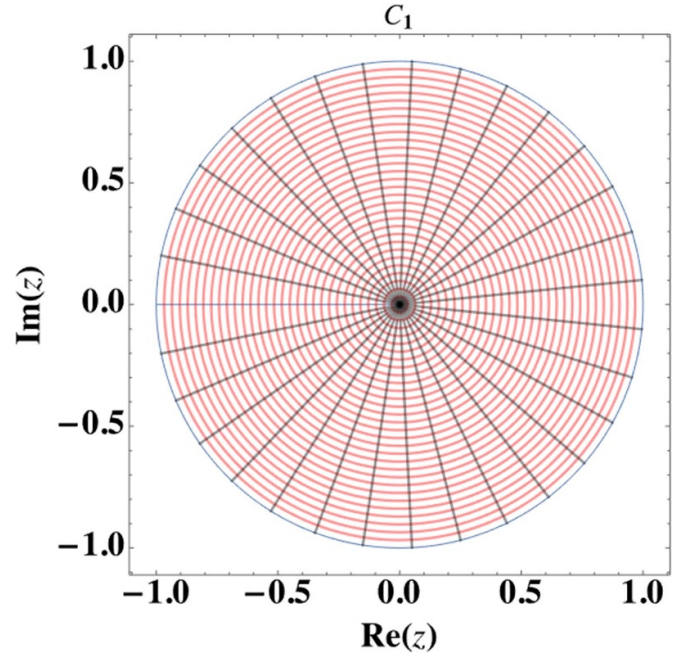


Figure 7. The complex plane \mathbb{C}_1 under the relation \triangleright (equation (37)) can be interpreted as each state z on a specific external ray is an element of the equivalence class, $[z]$. This leads to an isomorphism between \mathbb{C}_1 and S^1 (blue circle), and the distance between two equivalence classes $[z_1]$ and $[z_2]$ is given by the angular difference between the respective external rays (cf equation (36)). In this space, the distance between any two adjacent external rays depicted in the figure is the same.

embeddings in the complex plane with an additional structure given by the equivalence relation \triangleright on \mathbb{C} ,

$$z_1 \triangleright z_2 \text{ if } |z_1| = |R||z_2| \text{ and } \text{Arg}(z_1) = \text{Arg}(z_2) \quad (37)$$

where $|R|$ is a scale factor; i.e. z_1 and z_2 are on the same external ray. In addition, let us consider the mapping f defined by

$$\begin{aligned} f: \mathbb{C}_1 &\rightarrow \mathbb{C}_2 \\ z = re^{ik} &\mapsto w = f(z) = \frac{r}{2} e^{i\omega_k} \end{aligned} \quad (38)$$

where the indexes refer to the first and second copies of the complex plane, respectively. Therefore, if we consider the usual infinitesimal line element on \mathbb{C}

$$ds_{\mathbb{C}}^2 = dzdz^* = dr^2 + r^2 d\theta^2, \quad z = re^{i\theta} \quad (39)$$

where $*$ is the complex conjugate, we obtain that \mathbb{C}_1 and \mathbb{C}_2 under the relation \triangleright , are isomorphic to S^1 (see figure 7) and *FS* manifold (see figures 8 and 9), respectively.

Then, in figures 8 and 9(a)–(c), we show the maps \mathbb{C}_1 onto \mathbb{C}_2 under f given by equation (38) with different values $\bar{\epsilon}$ and λ ; a first observation is that f preserves circles and external rays only in the nontrivial topological regime, but deforms circles onto arcs of circles, given another geometrical perspective of equation (14). This mapping also allows for a visual realization of the inequality equation (35), in which $\text{vol}(\text{BZ})$

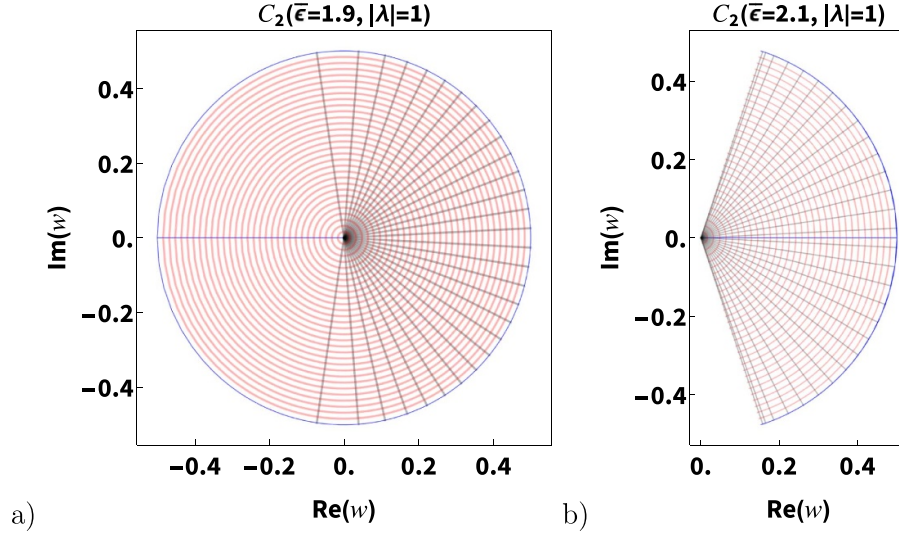


Figure 8. The image of \mathbb{C}_1 (figure 7) under the mapping f (equation (38)) with the values $|\lambda| = 1$ and (a) $\bar{\epsilon} = 1.9$, (b) $\bar{\epsilon} = 2.1$ are shown. In the nontrivial topological regime, $|\bar{\epsilon}| \leq 2$, f maps rays and circles from \mathbb{C}_1 (figure 7) to rays and circles with half the radius, respectively. On the other hand, in the trivial topological regime, circles are transformed into arcs of circles, providing another geometrical interpretation of equation (14). The inequality in equation (35) is visible in these figures. Thus, $\text{vol}(BZ)$ (cf equation (34)) corresponds to the perimeter of the blue circle (or the arc circle), respectively; therefore, in the topological regime, the equality holds (a), while in the nontopological regime (b) the strict inequality holds.

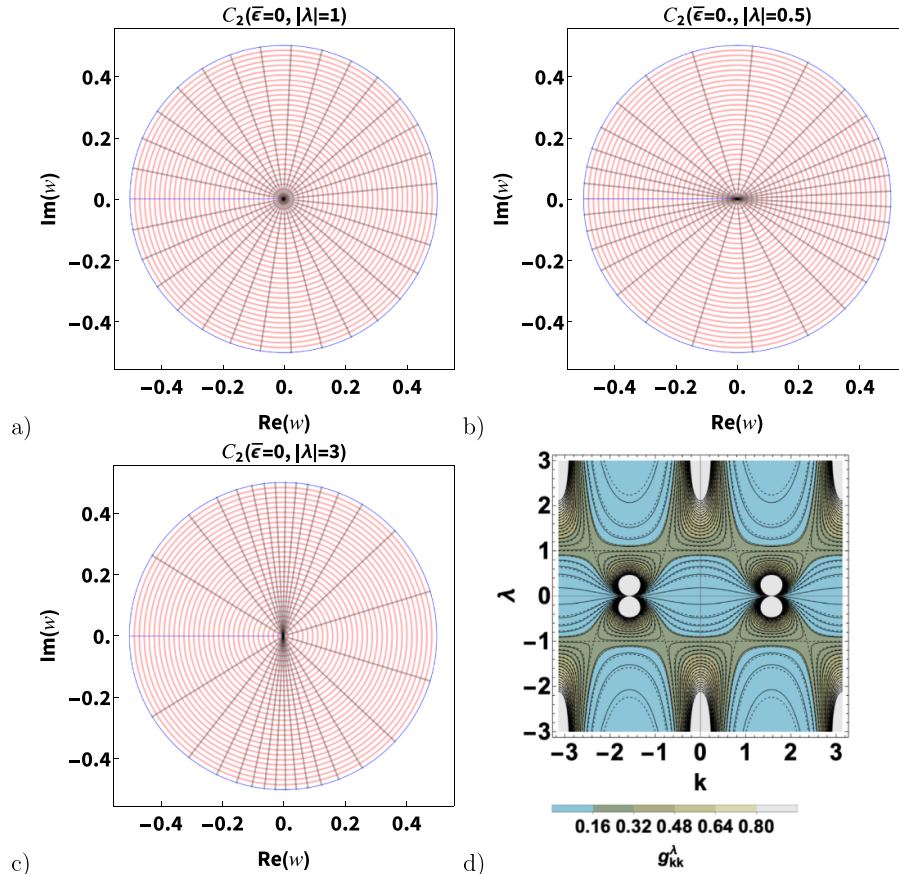


Figure 9. The image of \mathbb{C}_1 (figure 7) under the mapping f (equation (38)) with the values $\bar{\epsilon} = 0$ and (a) $|\lambda| = 1$, (b) $|\lambda| = 0.5$ and (c) $|\lambda| = 3$, and a contour plot of the metric tensor g_{kk}^{\pm} given by equation (32) as a function of λ and k with $\bar{\epsilon} = 0$ (d) are shown. As discussed, f preserves circles and external rays in the topological regime (see figure 8); however, it deforms the distribution of rays, which is related to the FS metric tensor, g_{kk}^{\pm} . For example, in the case of (c) where $|\lambda| = 3$, the external rays appear to separate near the angles $k = 0, \pm\pi$ and correspond to the maxima of g_{kk}^{\pm} as seen in (d). This geometric representation reveals that although all 3 systems have a nontrivial topology with $\nu = 1$, the FS metric allows us to distinguish between them. In particular, system (a), corresponding to the regime of FBs, is the only system in which the distribution of rays is preserved under f .

corresponds to the perimeter of the blue circle (or arc circle), respectively (see figure 8).

However, as we show in figures 9(a)–(c), f deform the distribution of rays, which is related to the FS metric tensor, g_{kk}^{\pm} . For example, in the case of figure 9(b) where $\lambda = 0.5$, the external rays appear to separate near the angles $k = \pm\pi/2$ and correspond to the maxima of g_{kk}^{\pm} as shown in figure 9(d). In a similar form, in the case of figure 9(c) where $\lambda = |3|$ for $k = 0, \pm\pi$. Something noteworthy about this geometric representation is that although all three systems have a nontrivial topology with $|\nu| = 1$, the FS metric allows us to establish differences between them. In particular, system figure 9(a) corresponding to the regime of FBs is the only system in which the distribution of rays is not deformed under f .

This can be confirmed as in the FB regime, the FS metric is constant as,

$$\partial_k \omega_k (\lambda = \pm 1) = \pm l \text{ (cf. 9)} \quad (40)$$

and thus is equivalent to the usual metric over S^1 . Such equivalence is readily found from the fact that an arc element ds of a geodesic in the FS manifold is given by,

$$ds_{FS}^2 = \left(\frac{l}{2}\right)^2 dk^2, \quad |k| \leq \pi/l \quad (41)$$

equivalent to an arc element of a circle with a radius $l/2$.

4. Conclusions

In conclusion, we have shown a mapping between a chain with $s-p$ orbitals onto a Kitaev–Creutz type model. With this map, we have found the existence of pseudo-Bogoliubov modes and CLSs in the FB regime, which obeys an analogous Landau relation (cf equation (17)). In addition, we obtained that there is a nontrivial topological transition by condition $\bar{\varepsilon} = \pm 2$ (see figure 3) that results in a nontrivial winding number. Furthermore, our analysis reveals the fingerprint of the FBs with the FS metric that allows us to distinguish between pure states of systems with the same topology; in particular, in this model, the FS metric is equivalent to the usual metric over S^1 in the FB regime. These findings could have implications for developing simpler models that aid understanding of FB formation and its effects on many-body interactions.

Data availability statement

All data that support the findings of this study are included within the article (and any supplementary files).

Acknowledgments

A J E C and G G N thanks the CONAHCyT fellowship (No. CVU 1007044) and the Universidad Nacional Autónoma de México (UNAM) for providing financial support. This work was supported by UNAM DGAPA PAPIIT IN102620 and CONAHCyT project 1564464.

Appendix. Bogoulibov transformation

We define the pseudo-Bogoulibov modes γ_k, ϱ_k as

$$\gamma_k \equiv u_k a_k + v_k b_k \text{ and } \varrho_k \equiv -v_k^* a_k + u_k^* b_k \quad (A.1)$$

and the anti-commutation relations for γ_k are

$$\begin{aligned} \{\gamma_k, \gamma_{k'}^\dagger\} &= (u_k a_k + v_k b_k) (u_{k'}^* a_{k'}^\dagger + v_{k'}^* b_{k'}^\dagger) \\ &\quad + (u_{k'}^* a_{k'}^\dagger + v_{k'}^* b_{k'}^\dagger) (u_k a_k + v_k b_k) \\ &= u_k u_{k'}^* \{a_k, a_{k'}^\dagger\} + v_k v_{k'}^* \{b_k, b_{k'}^\dagger\} \\ &\quad + u_k v_{k'}^* \{a_k, b_{k'}^\dagger\} + u_{k'}^* v_k \{b_k, a_{k'}^\dagger\} \\ &= (u_k u_{k'}^* + v_k v_{k'}^*) \delta_{kk'} \\ &= \delta_{kk'}, \text{ if } |u_k|^2 + |v_k|^2 = 1 \end{aligned} \quad (A.2)$$

$$\begin{aligned} \{\gamma_k, \gamma_{k'}\} &= (u_k a_k + v_k b_k) (u_{k'} a_{k'} + v_{k'} b_{k'}) \\ &\quad + (u_{k'} a_{k'} + v_{k'} b_{k'}) (u_k a_k + v_k b_k) \\ &= u_k u_{k'} \{a_k, a_{k'}\} + v_k v_{k'} \{b_k, b_{k'}\} \\ &\quad + u_k v_{k'} \{a_k, b_{k'}\} + u_{k'} v_k \{b_k, a_{k'}\} \end{aligned} \quad (A.3)$$

$$= 0 \quad (A.4)$$

$$\begin{aligned} \{\gamma_k^\dagger, \gamma_{k'}^\dagger\} &= (u_k^* a_k^\dagger + v_k^* b_k^\dagger) (u_{k'}^* a_{k'}^\dagger + v_{k'}^* b_{k'}^\dagger) \\ &\quad + (u_{k'}^* a_{k'}^\dagger + v_{k'}^* b_{k'}^\dagger) (u_k^* a_k^\dagger + v_k^* b_k^\dagger) \\ &= u_k^* u_{k'}^* \{a_k^\dagger, a_{k'}^\dagger\} + v_k^* v_{k'}^* \{b_k^\dagger, b_{k'}^\dagger\} \\ &\quad + u_k^* v_{k'}^* \{a_k^\dagger, b_{k'}^\dagger\} + u_{k'}^* v_k^* \{b_k^\dagger, a_{k'}^\dagger\} \end{aligned} \quad (A.5)$$

$$= 0 \quad (A.6)$$

and similar anticommutation relations for ϱ_k under the interchange of $u_k \leftrightarrow -v_k^*$ and $v_k \leftrightarrow u_k^*$. From the definition, (A.1) we can obtain the following result


$$\begin{aligned} \epsilon(k) (\gamma_k^\dagger \gamma_k - \varrho_k^\dagger \varrho_k) &= \epsilon(k) \left[(u_k^* a_k^\dagger + v_k^* b_k^\dagger) (u_k a_k + v_k b_k) \right. \\ &\quad \left. - (-v_k a_k^\dagger + u_k b_k^\dagger) (-v_k^* a_k + u_k^* b_k) \right] \\ &= \epsilon(k) \left[(|u_k|^2 - |v_k|^2) a_k^\dagger a_k \right. \\ &\quad \left. + (|u_k|^2 - |v_k|^2) b_k^\dagger b_k + 2u_k^* v_k a_k^\dagger b_k \right. \\ &\quad \left. + 2u_k v_k^* b_k^\dagger a_k \right]. \end{aligned} \quad (A.7)$$

If we choose u_k and v_k as $u_k \equiv \cos(\frac{\omega_k}{2})$, $v_k \equiv -i \sin(\frac{\omega_k}{2})$ where

$$\begin{aligned} \sin(\omega_k) &\equiv \frac{2\lambda \sin(kl)}{\epsilon(k)}, \quad \cos(\omega_k) \equiv \frac{\bar{\varepsilon} + 2 \cos(kl)}{\epsilon(k)}, \\ \epsilon(k) &= \sqrt{(\bar{\varepsilon} + 2 \cos(kl))^2 + (2\lambda \sin(kl))^2}. \end{aligned} \quad (A.8)$$

We recover the Hamiltonian form of equation (5). We note that only in the two cases $\bar{\varepsilon} = 0, \lambda = \pm 1$, the relation ω_k with k is linear, that is, $\omega_k = \pm kl$, if $\lambda = \pm 1$ and $\bar{\varepsilon} = 0$.

ORCID iDs

Abdiel de Jesús Espinosa-Champo  <https://orcid.org/0000-0001-6849-9686>

Gerardo G Naumis  <https://orcid.org/0000-0002-1338-1522>

References

- [1] Leykam D, Andreanov A and Flach S 2018 *Adv. Phys. X* **3** 1473052
- [2] Bergholtz E J and Liu Z 2013 *Int. J. Mod. Phys. B* **27** 1330017
- [3] Nguyen H S, Dubois F, Deschamps T, Cuff S, Pardon A, Leclercq J L, Seassal C, Letartre X and Viktorovitch P 2018 *Phys. Rev. Lett.* **120** 066102
- [4] Deng S, Simon A and Köhler J 2003 *J. Solid State Chem.* **176** 412–6
- [5] Qiu W X, Li S, Gao J H, Zhou Y and Zhang F C 2016 *Phys. Rev. B* **94** 241409
- [6] Drost R, Ojanen T, Harju A and Liljeroth P 2017 *Nat. Phys.* **13** 668–71
- [7] Abilio C C, Butaud P, Fournier T, Pannetier B, Vidal J, Tedesco S and Dalzotto B 1999 *Phys. Rev. Lett.* **83** 5102–5
- [8] Taie S, Ozawa H, Ichinose T, Nishio T, Nakajima S and Takahashi Y 2015 *Sci. Adv.* **1** e1500854
- [9] Nakata Y, Okada T, Nakanishi T and Kitano M 2012 *Phys. Rev. B* **85** 205128
- [10] He Y, Mao R, Cai H, Zhang J X, Li Y, Yuan L, Zhu S Y and Wang D W 2021 *Phys. Rev. Lett.* **126** 103601
- [11] Naumis G G, Navarro-Labastida L A, Aguilar-Méndez E and Espinosa-Champo A 2021 *Phys. Rev. B* **103** 245418
- [12] Navarro-Labastida L A, Espinosa-Champo A, Aguilar-Mendez E and Naumis G G 2022 *Phys. Rev. B* **105** 115434
- [13] Mielke A and Tasaki H 1993 *Commun. Math. Phys.* **158** 341–71
- [14] Tasaki H 1998 *Prog. Theor. Phys.* **99** 489–548
- [15] Cao Y, Fatemi V, Fang S, Watanabe K, Taniguchi T, Kaxiras E and Jarillo-Herrero P 2018 *Nature* **556** 43–50
- [16] Aoki H 2020 *J. Supercond. Nov. Magn.* **33** 2341–6
- [17] Wu C, Bergman D, Balents L and Das Sarma S 2007 *Phys. Rev. Lett.* **99** 070401
- [18] Jaworowski B, Güçlü A D, Kaczmarkiewicz P, Kupczyński M, Potasz P and Wójs A 2018 *New J. Phys.* **20** 063023
- [19] Settle M, Engelen R, Salib M, Michaeli A, Kuipers L and Krauss T 2007 *Opt. Express* **15** 219–26
- [20] Krauss T F 2007 *J. Phys. D: Appl. Phys.* **40** 2666
- [21] Mandilara A, Valagiannopoulos C and Akulin V M 2019 *Phys. Rev. A* **99** 023849
- [22] Sarsen A and Valagiannopoulos C 2019 *Phys. Rev. B* **99** 115304
- [23] Mielke A 1991 *J. Phys. A: Math. Gen.* **24** L73
- [24] Tasaki H 1992 *Phys. Rev. Lett.* **69** 1608–11
- [25] Shima N and Aoki H 1993 *Phys. Rev. Lett.* **71** 4389–92
- [26] Aoki H, Ando M and Matsumura H 1996 *Phys. Rev. B* **54** R17296–9
- [27] Kerelsky A *et al* 2021 *Proc. Natl Acad. Sci.* **118** e2017366118
- [28] Sutherland B 1986 *Phys. Rev. B* **34** 5208–11
- [29] Lieb E H 1989 *Phys. Rev. Lett.* **62** 1201–4
- [30] Zheng L, Feng L and Yong-Zhi W 2014 *Chin. Phys. B* **23** 077308
- [31] Thouless D J, Kohmoto M, Nightingale M P and den Nijs M 1982 *Phys. Rev. Lett.* **49** 405–8
- [32] Regnault N and Bernevig B A 2011 *Phys. Rev. X* **1** 021014
- [33] Parameswaran S A, Roy R and Sondhi S L 2013 *C. R. Physique* **14** 816–39
- [34] Li Z *et al* 2018 *Sci. Adv.* **4** eaau4511
- [35] Laughlin R B 1983 *Phys. Rev. Lett.* **50** 1395–8
- [36] Ledwith P J, Khalaf E and Vishwanath A 2021 *Ann. Phys., NY* **435** 168646
- [37] Mera B and Ozawa T 2021 *Phys. Rev. B* **104** 115160
- [38] Mera B and Ozawa T 2021 *Phys. Rev. B* **104** 045104
- [39] Ozawa T and Mera B 2021 *Phys. Rev. B* **104** 045103
- [40] Li Y, Yuan Q, Guo D, Lou C, Cui X, Mei G, Petek H, Cao L, Ji W and Feng M 2023 *Adv. Mater.* **35** 2300572
- [41] Seenithurai S and Chai J D 2018 *Sci. Rep.* **8** 13538
- [42] Kochat V *et al* 2018 *Sci. Adv.* **4** e1701373
- [43] Ishtiyak M, Panigrahi G, Jana S, Prakash J, Mesbah A, Malliakas C D, Lebègue S and Ibers J A 2020 *Inorg. Chem.* **59** 2434–42
- [44] Harrison W 1989 *Electronic Structure and the Properties of Solids: The Physics of the Chemical Bond (Dover Books on Physics)* (Dover)
- [45] Jünemann J, Piga A, Ran S J, Lewenstein M, Rizzi M and Bermudez A 2017 *Phys. Rev. X* **7** 031057
- [46] Kuno Y, Orito T and Ichinose I 2020 *New J. Phys.* **22** 013032
- [47] Kang J H, Han J H and Shin Y 2020 *New J. Phys.* **22** 013023
- [48] Mukherjee A, Nandy A, Sil S and Chakrabarti A 2022 *Phys. Rev. B* **105** 035428
- [49] Shi Y H *et al* 2023 *Phys. Rev. Lett.* **131** 080401
- [50] Girvin S M and Yang K 2019 *Modern Condensed Matter Physics* (Cambridge University Press)
- [51] Thirulogasanthar K and Muraleetharan B 2018 Canonical, squeezed and fermionic coherent states in a right quaternionic Hilbert space with a left multiplication on it *Coherent States and Their Applications* ed J P Antoine, F Bagarello and J P Gazeau (Springer) pp 135–55
- [52] Navarro-Labastida L A and Naumis G G 2023 *Phys. Rev. B* **107** 155428
- [53] Leumer N, Marganska M, Muralidharan B and Grifoni M 2020 *J. Phys.: Condens. Matter* **32** 445502
- [54] Altland A and Zirnbauer M R 1997 *Phys. Rev. B* **55** 1142–61
- [55] Kempkes S N, Slot M R, van den Broeke J J, Capiod P, Benalcazar W A, Vanmaekelbergh D, Bercioux D, Swart I and Morais Smith C 2019 *Nat. Mater.* **18** 1292–7
- [56] Chiu C K, Teo J C Y, Schnyder A P and Ryu S 2016 *Rev. Mod. Phys.* **88** 035005
- [57] Rhim J W and Yang B J 2021 *Adv. Phys. X* **6** 1901606
- [58] Andrade E, López-Urías F and Naumis G G 2023 *Phys. Rev. B* **107** 235143
- [59] Matsumoto D, Mizoguchi T and Hatsugai Y 2023 *J. Phys. Soc. Japan* **92** 034705
- [60] Yoshida T, Mizoguchi T, Kuno Y and Hatsugai Y 2021 *Phys. Rev. B* **103** 235130
- [61] Mizoguchi T, Kuno Y and Hatsugai Y 2023 arXiv:2308.03971
- [62] Mizoguchi T and Hatsugai Y 2023 *Phys. Rev. B* **107** 094201
- [63] Naumis G G 2007 *Phys. Rev. B* **76** 153403
- [64] Barrios-Vargas J E and Naumis G G 2011 *J. Phys.: Condens. Matter* **23** 375501
- [65] Kane C L and Lubensky T C 2014 *Nat. Phys.* **10** 39–45
- [66] Phillips J 1979 *J. Non-Cryst. Solids* **34** 153–81
- [67] Huerta A and Naumis G G 2002 *Phys. Rev. B* **66** 184204
- [68] Flores-Ruiz H M and Naumis G G 2011 *Phys. Rev. B* **83** 184204
- [69] Ozawa T and Goldman N 2018 *Phys. Rev. B* **97** 201117
- [70] Julku A, Bruun G M and Törmä P 2021 *Phys. Rev. B* **104** 144507
- [71] Cayssol J and Fuchs J N 2021 *J. Phys. Mater.* **4** 034007
- [72] Kruchkov A 2022 *Phys. Rev. B* **105** L241102
- [73] Huhtinen K E, Herzog-Arbeitman J, Chew A, Bernevig B A and Törmä P 2022 *Phys. Rev. B* **106** 014518
- [74] Ozawa T and Goldman N 2019 *Phys. Rev. Res.* **1** 032019

- [75] Bengtsson I and Zyczkowski K 2006 *Geometry of Quantum States: An Introduction to Quantum Entanglement* (Cambridge University Press)
- [76] Cheng R 2013 Quantum geometric tensor (fubini-study metric) in simple quantum system: a pedagogical introduction (arXiv:[1012.1337](https://arxiv.org/abs/1012.1337))
- [77] Mera B, Zhang A and Goldman N 2022 *SciPost. Phys.* **12** 018
- [78] Peotta S and Törmä P 2015 *Nat. Commun.* **6** 8944
- [79] Julku A, Peotta S, Vanhala T I, Kim D H and Törmä P 2016 *Phys. Rev. Lett.* **117** 045303
- [80] Tovmasyan M, Peotta S, Törmä P and Huber S D 2016 *Phys. Rev. B* **94** 245149
- [81] Xie F, Song Z, Lian B and Bernevig B A 2020 *Phys. Rev. Lett.* **124** 167002
- [82] Herzog-Arbeitman J, Peri V, Schindler F, Huber S D and Bernevig B A 2022 *Phys. Rev. Lett.* **128** 087002
- [83] Herzog-Arbeitman J, Chew A, Huhtinen K E, Törmä P and Bernevig B A 2022 Many-body superconductivity in topological flat bands (arXiv:[2209.00007](https://arxiv.org/abs/2209.00007))